HHS Public Access

Author manuscript

Ann Biomed Eng. Author manuscript; available in PMC 2017 March 30.

Published in final edited form as:

Ann Biomed Eng. 2015 December ; 43(12): 2978–2990. doi:10.1007/s10439-015-1353-0.

Transdermal Delivery of Functional Collagen *Via* Polyvinylpyrrolidone Microneedles

Wenchao Sun[1,2], **Mohammed Inayathullah**[1,2], **Martin A. C. Manoukian**[1,3], **Andrey V. Malkovskiy**[1], **Sathish Manickam**[1], **M. Peter Marinkovich**[3,4], **Alfred T. Lane**[3], **Lobat Tayebi**[5,1], **Alexander M. Seifalian**[6], and **Jayakumar Rajadas**[1,2]

[1]Biomaterials and Advanced Drug Delivery Laboratory, Stanford University School of Medicine, 1050 Arastradero Road, Building A, Room A148, Palo Alto, CA 94304, USA

[2]Cardiovascular Pharmacology Division, Cardiovascular Institute, Stanford University School of Medicine, Stanford, CA 94305, USA

[3]Department of Dermatology, Stanford University School of Medicine, Stanford, CA 94305, USA

[4]Division of Dermatology, Palo Alto VA Medical Center, Palo Alto, CA 94304, USA

[5]Department of Developmental Sciences, Marquette University School of Dentistry, Milwaukee, WI 53201, USA

[6]Division of Surgery and Interventional Science, University College London, London, UK

Abstract

Collagen makes up a large proportion of the human body, particularly the skin. As the body ages, collagen content decreases, resulting in wrinkled skin and decreased wound healing capabilities. This paper presents a method of delivering type I collagen into porcine and human skin utilizing a polyvinylpyrrolidone microneedle delivery system. The microneedle patches were made with concentrations of 1, 2, 4, and 8% type I collagen (w/w). Microneedle structures and the distribution of collagen were characterized using scanning electron microscopy and confocal microscopy. Patches were then applied on the porcine and human skin, and their effectiveness was examined using fluorescence microscopy. The results illustrate that this microneedle delivery system is effective in delivering collagen I into the epidermis and dermis of porcine and human skin. Since the technique presented in this paper is quick, safe, effective and easy, it can be considered as a new collagen delivery method for cosmetic and therapeutic applications.

Address correspondence to Jayakumar Rajadas, Cardiovascular Pharmacology Division, Cardiovascular Institute, Stanford University School of Medicine, Stanford, CA 94305, USA. jayraja@stanford.edu.
Wenchao Sun and Mohammed Inayathullah contributed equally to this work.

ELECTRONIC SUPPLEMENTARY MATERIAL

The online version of this article (doi:10.1007/s10439- 015-1353-0) contains supplementary material, which is available to authorized users.

CONFLICT OF INTEREST

AT.L., M.P.M., and J.R. are listed on the following patent assigned to Stanford University: Production and delivery of a stable collagen (WO 2012149136).

Keywords

Collagen; Microneedles; Biomaterials; Transdermal delivery

INTRODUCTION

The human body is composed of 20% proteins by mass, and 25–35% of total protein is represented by collagen, of which roughly 90% is type I collagen (C1).[7] C1 contributes to the make-up of many types of tissue within the human body, including skin, tendon, teeth, bone, and endothelial lining. Deficits of C1 can lead to numerous negative outcomes, from cosmetic blemishes such as wrinkles and decreased ability of wound healing, to life altering and debilitating diseases, such as Osteogenesis Imperfecta and Ehler– Danlos Syndrome.[6,23,33] These deficits can be caused by congenital defects, infection, autoimmune diseases, nutrient deficiency, sun damage, or old age.[4,20,26] Aging alone can reduce the collagen content of adult human skin to 1% per unit area per year.[27] This decrease is due in large part to the formation of free radicals, which accelerate enzymatic degradation of the dermal layers and inhibit synthesis of collagen fibers. Increased iron levels have been shown to increase the sensitivity of fibroblasts and keratinocytes to UVA light, leading to upregulation of matrix metallopeptidase 1 and playing a major role in skin photoaging, especially among post-menopausal women.[14]

Different approaches have been employed to introduce C1 into the skin to treat cosmetic blemishes and contribute in the wound repair process. Commonly, cosmetic collagen introduction has been performed using syringe injections; whereas collagen based bandages have been utilized to assist in wound healing[3,9,25] Though these methods have proven to be effective, they include many drawbacks. The use of syringes is accompanied by the risk of an accidental stabbing which may result in injury that is highly destructive to facial tissue. This could negate the commercial benefit of injecting collagen into sensitive areas such as lips and lines around the mouth. Additionally, a syringe can only introduce C1 into the skin in large scale and globular forms, which does not always provide the adequate distribution of collagen necessary for homogenous skin plumpness and wrinkle repair. On the other hand, though collagen bandages have been shown to increase fibroblast recruitment to trauma areas, they can only be applied superficially, restricting their effectiveness.

Various techniques of microneedle delivery have been created utilizing solid, hollow, and dissolvable tips.[17] Microneedles have illustrated their ability to transdermally (and ocularly) deliver various molecules in a targeted manner using injectable, drug coated metal or polymer microneedles.[1,10,13,19,22] Metal microneedles rollers (Dermaroller) have been shown to induce C1 deposition in Murine skin.[16] However, there has been no attempt made for the use of microneedles as a delivery system for C1 into human skin. We have previously demonstrated the delivering of allergen molecules into human foreskin.[30] In the present study, we prepared a dissolvable polymeric microneedle for transdermal delivery of C1.

A dissolvable C1 microneedle delivery system is superior to the use of syringes or bandages for both cosmetic and wound treatment purposes. Dissolvable microneedles can eliminate the danger of sharps that is present when using syringes. This would make C1 application

simpler and easier, allowing for self-application within one's own home, which could open up a potentially lucrative market for at-home C1 delivery. Moreover, a microneedle delivery system would allow even distribution of C1 throughout the application zone, eliminating the threat of globular distribution. This effectively contributes to an even and natural look to the skin, instead of the bulbous look that may result from syringe injections.

In addition to the increased cosmetic benefits, the use of a microneedle delivery system would greatly benefit the wound healing process. Dissolvable microneedles can penetrate into the skin perpendicularly, instead of parallel administration of collagen in bandages. Such intradermal perpendicular scaffolding has been shown to increase the rate of wound healing in which fibroblasts are recruited, helping to rapidly heal trauma to the skin.[15] In the present study, we have utilized porcine skin, a well-accepted adult human skin analogue, and human foreskin to illustrate the effectiveness of employing polyvinylpyrrolidone microneedles for transdermal delivery of C1.

MATERIALS AND METHODS

Preparation of PDMS Negative Mold

PDMS molds were fabricated as reported previously. [30] In short, a silicon wafer (1 mm thick, 100 mm in diameter) with oxide mask was patterned using standard contact lithographic techniques with thick photoresist and subjected to deep reactive ion etching. The residual photoresist was removed using oxygen plasma and the wafers were washed in sulfuric acid. The silicon wafer was diced into ~0.6 × 0.6 cm squares with 12 × 12, 12 × 6 or 6 × 6 needle arrays. To facilitate easy removal of molded materials, all wafers were silanized overnight in a vacuum chamber prior to use. To prepare PDMS mold, dimethylsiloxane monomer and curing agent (10:1 w/w, Dow Corning, Midland, MI) were mixed and poured onto silicon positive mold in a sterile Petri dish. To remove bubbles of trapped air, a vacuum was applied for 5 min. To cure the PDMS, the Petri dish was incubated at 37 °C overnight.

Labeling of Collagen I with Fluorophores

C1 (~10 mg/mL) from rat tail tendon (Corning Inc, Cat# 354249) was dialyzed against 50 mM MES buffer (pH 6.0). 25 μL of 10 mg/mL rhodamine B isothiocyanate (RBITC) (Sigma-Aldrich Cat# 283924) in DMF was diluted with 50 mM MES buffer (pH 6.0) to a total volume of 0.5 mL and added dropwise to 6 mL of 4 mg/mL C1 in 50 mM MES buffer (pH 6.0). Reaction was kept at 4 °C for 4 h in the dark with stirring. Reaction mixture was then dialyzed at 4 °C in the dark against 50 mM MES buffer (pH 6.0) to remove unreacted RBITC.

Preparation of Microneedle Patches

Polyvinylpyrrolidone (PVP) (MW = 10 kDa) (Sigma- Aldrich, Cat# PVP10-500G) was dissolved in water to form solutions containing concentrations of 133.38, 266.76, and 533.52 mg/mL PVP. Poly ethylene glycol- 400 (PEG) (Sigma-Aldrich, Cat# 202398), a plasticizer, was added to the PVP solutions in a ratio of 10 μL PEG/ 200 mg PVP. C1 was mixed with 50 mM MES buffer (pH 6.0) to create final solutions containing 10, 8, and 4 mg/mL C1. For the 1%C1microneedle patch, 370 μL of 133.38 mg/mL PVP/PEG solution was mixed with

125 μL of 4 mg/mL C1 solution. For the 2% C1 microneedle patch, 367.4 μL of 133.38 mg/mL PVP/PEG solution was mixed with 125 μL of 8 mg/mL C1 solution. For the 4% C1 microneedle patch, 179.98 μL of 266.76 mg/mL PVP/PEG solution was mixed with 250 μL of 8 mg/mL C1 solution. For the 8% C1 patch, 86.2 μL of 533.52 mg/mL PVP/PEG solution was mixed with 400 μL of 10 mg/mL C1 solution. 1% rhodamine labeled C1 was used to prepare fluorescently labeled 1% C1 microneedle. For fluorescently labeled 2, 4, 8% C1 microneedles, 1%rhodamine labeled C1 was mixed with unlabeled C1 to reach the final concentrations.

PVP/C1 solutions (50 μL) were then pipetted onto PMDS mold (~0.6 cm × 0.6 cm). The mold was placed in a vacuum to force the liquid into the needle chambers. Air bubbles were removed using a pipette tip. After the solution was allowed to air dry for 4–5 h, another 50 μL of PVP/C1 solution was added. The solution on the mold was allowed to dry overnight before addition of the final 70 μL of PVP/C1 solution. After drying, the microneedle patches were then peeled from the mold using an adhesive tape.

Characterization by Scanning Electron Microscopy (SEM) and Confocal Fluorescence Microscopy

Microneedle morphology was examined by scanning electron microscopy (SEM). The microneedles along with their bases were attached to an SEM sample stub using a double-stick carbon tab. The samples were coated with a 7 nm thick gold–palladium layer using a Denton Desk II vacuum sputter coater. Imaging was carried out on a Hitachi S-3400 N VP scanning electron microscope at the Cell Sciences Imaging Facility, Stanford University. C1 distribution inside the microneedles was examined by confocal fluorescence microscopy. Rhodamine labeled 1% C1 microneedles were secured in embedding resin and imaged by Leica SP5 upright confocal fluorescence microscope.

Electron Beam (e-beam) Sterilization

100 μL of ~10 mg/mL naked C1 in 50 mM MES buffer (pH 6.0) was air dried at room temperature. Naked C1 and C1 microneedles were placed in a sealed plastic bag containing desiccant and shipped at ambient temperature to Nutek Corporation (Hayward, CA) for e-beam treatment. A split dose of 12.5 + 12.5 kGy was used with sample freezing before, between and after passes.

SDS-PAGE Analysis of Collagen

The collagen microneedles treated or untreated with e-beam were dissolved in excess 50 mMMES buffer (pH 6.0) and washed three times with MES buffer using a 30,000 MWCO Vivaspin 20 filter (Sartorius) in a refrigerated centrifuge to remove PVP. To completely solubilize collagen, the washing was continued for additional three times using 0.02 Nacetic acid. Air dried naked C1, treated or untreated with e-beam were redissolved in 0.02 N acetic acid. C1 concentration was determined using the Pierce BCA protein assay (Thermo Scientific Cat# 23227) with the original C1 in 0.02 N acetic acid (Corning Inc, Cat# 354249) as calibration standard. We typically recover >95% of the input. 1.5 μg of collagen in LDS sample buffer (Life Technologies) with reducing agent was loaded onto a Nu- PAGE 4–12%

bis tris gel (Life Technologies). After electrophoresis, the gel was washed in distilled water and stained with SimplyBlue SafeStain (Life Technologies).

Enzyme-Linked Immunosorbent assay (ELISA) to Determine Concentration of Functional Collagen

Naked C1 and C1 in microneedles were recovered as described above. Rat Type I Collagen Detection Kit (Chondrex Inc, Cat# 6013) was used to determine the concentration of functional C1. All samples were diluted to 2 μg/mL using the Sample/Standard Dilution Buffer (Solution B) provided in the kit. ELISA was performed according to manufacturer's instruction. For each condition, three samples were tested with assay duplicate for each sample.

Circular Dichroism (CD) Spectra of Collagen Recovered from Microneedles

Naked C1 and C1 in microneedles were recovered as described in the SDS-PAGE experiment. The collagen solution was diluted in 0.02 N acetic acid to 0.1 mg/ mL and placed into a 0.1 cm path length quartz cell. Spectra were acquired using a Jasco Model J-810 spectropolarimeter (Jasco, Japan) from ≈190 to 260 nm with a scan rate of 100 nm/ min. The CD data represent averages from five recordings and was processed for routine baseline correction and subtraction of buffer spectra according to the manufacturer's instructions. For samples that had traces of PVP, high photomultiplier voltage at low wavelength precluded data acquisition to wavelengths as low as 190 nm.

Porcine Skin Penetration and Microscopic Examination of Fluorescence

Cadaver porcine skin was obtained from euthanized pigs that had been used in previous cardiac experiments at Stanford. The skin was collected after the pig had been euthanized according to the approved Stanford Administrative Panel on Laboratory Animal Care guidelines. Porcine skin was cut into a ~2 cm × 2 cm square and placed on a piece of glass with epidermis facing up. A small patch of fluorescently labeled C1 microneedle patch (~0.6 cm × 0.6 cm) was applied onto the skin and secured in place with a Tegaderm dressing (3 M). The microneedle patch was pressed down using a small Petri dish for 30 s. After 15 min, the Tegaderm was removed and the skin was gently stripped with another clean Tegaderm to remove any residue on the surface. For low magnification fluorescent needle marker imaging, the skin was imaged using a fluorescence stereomicroscope (Leica M165 FC with DSR filter). For Trypan blue staining, Trypan blue was applied to skin surface and incubated for 1 min. After gentle washing of the skin surface, pictures were taken using a stereomicroscope (Leica M165 FC). For fluorescence imaging of skin sections, the skin was immersed in 4% paraformaldehyde and fixed overnight. Fixed skin was embedded in optimum cutting temperature (OCT) compound (Fisher HealthCare) on dry ice and cryosectioned. Tissue slides were preserved in mounting medium with DAPI (4′,6-diamidino-2- phenylindole) (Vector Labs) and examined with fluorescence microscopy.

Foreskin Penetration and Microscopic Examination of Fluorescence

Human foreskin was obtained from discarded neonatal foreskins obtained after elective circumcision. Institutional Review Board approval was obtained prior to tissue collection.

The sample was cut into a ~2 cm × 2 cm square, stretched and pinned onto a Styrofoam board with epidermis facing up. A small patch of fluorescently labeled 1% collagen microneedle patch (~0.6 cm × 0.6 cm 12 × 12 array) was applied onto the skin and secured in place with a Tegaderm dressing. The microneedle patch was pressed down using a small Petri dish for 30 s. After 15 min, the Tegaderm was removed and the skin was gently stripped with another clean Tegaderm to remove any residue on the surface. Still pinned on the styrofoam, the skin was immersed in 4% paraformaldehyde and fixed overnight. Fixed skin was embedded in OCT compound on dry ice and cryosectioned. For laminin 332 immunofluorescence staining, a rabbit polyclonal antibody to laminin 332 (pKaL) from Marinkovich lab (Stanford University) was used at 1:400 dilution. Goat anti-rabbit IgG Alexa Fluor 488 secondary antibody (Life Technologies) was used at 1:500 dilution. Tissue slides were preserved in mounting medium with DAPI and observed using a fluorescence microscopy.

RESULTS

Characterization of Microneedles

Bright field imaging was used to illustrate the distribution of microneedles within the microneedle patch (Fig. 1a). A typical microneedle patch measures at 0.6 cm × 0.6 cm with an array of 12 × 12 needles. The microneedles were spaced about 500 μm apart, with each needle measuring approximately 365 μm in height and 135 μm in diameter at the base (Fig. 1b). The microneedles are tapered at the tips. This is consistent with the dimension of the silicon positive mold used to manufacture the polymer microneedles (Fig. 1c). The microneedle patches with 1, 2, 4, 8% (w/w) of C1 were prepared and inspected using SEM to study the morphology and surface characteristics (Fig. 2). A similar rough surface feature was observed for 1, 2, 4% C1 microneedles. This pattern was formed by replicating the surface feature of the silicon positive mold as the same pattern was seen for the silicon microneedles (Fig. 2 top panels). At 8% C1, the surface displayed a slightly different fibrous feature, possibly due to the formation of more fibrous aggregates by higher concentrations of collagen. Regardless of the collagen concentrations, the microneedle surface became smoothened after extended exposure in the air (1 h) (Supplementary Figure S1). This is mainly due to the hygroscopic property of PVP. For this reason, all the microneedle patches were stored in vacuum or with desiccant. However, within 1 h, the needles remained sharp (Supplementary Figure S1) which allows enough time to perform the different experimental procedures. At higher concentrations of C1, we also found more defective microneedles (Supplementary Figure S1 8%), indicating higher concentration of collagen may affect the mechanical strength of the microneedles.

To study the distribution of C1 inside the microneedles, microneedles with fluorescently labeled C1 (1%) were embedded in a resin block and imaged by confocal fluorescence microscopy. Optical sections of individual microneedles showed that C1 were uniformly distributed across the horizontal plane (Fig. 3). Vertical sections of the needles indicated that C1 were slightly more concentrated toward the tips of the needles, possibly due to aggregation at the tips.

Stability of C1 in Microneedle Patches After Electron Beam Sterilization

For C1 microneedle to be considered for potential commercial use, a proper sterilization procedure needs to be studied. With faster turnaround, less material degradation and lower cost compared to gamma irradiation, electron beam sterilization (e-beam) has become a commercially proven procedure for sterilizing a wide variety of medical products. We therefore chose e-beam technology to sterilize C1 microneedle. As control, naked C1 in 50 mM MES buffer (pH 6.0) was air dried at room temperature. After e-beam treatment, naked C1 was redissolved and C1 in microneedles were recovered as described in the Method section. The stability of C1 was first checked with protein gel electrophoresis. As shown in Fig. 4(a), no degradation was observed when C1 was air dried or recovered from microneedles without e-beam treatment. Some degradation was observed when C1 was treated with e-beam. Densitometry of the gel image indicated that after e-beam treatment, undegraded form of collagen reduced to 80.8 ± 2.1% (mean ± SD) compared to untreated control when C1 was incorporated in microneedles. However, ~38% of naked C1 protein (compared to untreated control) was degraded after e-beam treatment, indicating that collagen was protected in the microneedle from the damage caused by e-beam. The major bands representing the monomer α1 (I) and α2 (I) can be observed for all the samples. There is also no increase of the dimeric (β) or oligomeric from of C1 after e-beam treatment, indicating no additional crosslinking was caused by e-beam treatment. We confirmed the structural integrity of recovered C1 using circular dichroism (CD) spectroscopy which is an excellent technique to determine the conformation of proteins and peptides in solution.[12] The CD spectrum of the untreated native C1 showed a signature positive peak at 222 nm and a signature negative peak at ≈198 nm (Fig. 4c). These peaks were diminished when C1 was denatured by heating (Fig. 4c). When air dried naked C1 was treated by e-beam, a small decrease of the two peaks were observed indicating a partial loss of the triple-helical structure (Fig. 4d). C1 recovered from the microneedle without e-beam treatment showed similar CD spectra compared to untreated control indicating that C1 retained its native triple-helical conformation in PVP microneedles (Fig. 4e). After e-beam treatment, C1 recovered from the microneedle maintained the overall spectra, but also showed a partial loss of the triplehelical structure, especially at lower percentage of C1 (Fig. 4f). To test whether C1 recovered from microneedle maintained its function with or without e-beam treatment, an ELISA specific to rat type I collagen was performed. Prior to ELISA experiment, C1 concentration was determined using a BCA protein assay with the original C1 in 0.02 N acetic acid as calibration standard. Naked C1 and C1 recovered from microneedles were diluted to 2 μg/mL for the ELISA. Because the standard collagen solution provided in the ELISA kit was from a different source, the overall concentrations determined by the ELISA were higher than the value determined by the BCA assay. For this reason, the concentrations of functional collagen of all the samples were compared to the level of untreated control and the results were expressed as percent functional collagen. After heating the collagen at 90 °C for 5 min, no functional collagen could be detected, confirming the specificity of the assay (data not shown). As shown in Fig. 4(b), for C1 recovered from microneedles, ~80–90% of protein remained active. After e-beam treatment, there is a small decrease of functional collagen concentration compared to no e-beam treatment at 1, 2, 4% C1 (not statistically significant). In contrast, for air dried naked collagen, a more significant loss of function was observed. After e-beam treatment, only

64% of naked collagen remained active ($P<0.05$ when compared to all other samples except for naked C1 without e-beam which is not significant). This result is consistent with the SDS-PAGE and CD results and further confirms that more than 80% of C1 remained stable and functional in the microneedle and the incorporation protected C1 from the damage caused by e-beam.

Porcine Skin Collagen I Application

Porcine skin was used *in vitro* to test the penetrative and dissolvable properties of the microneedles due to its likeness to adult human skin.[2,5,8] Dissolution kinetics of the microneedles (1% rhodamine labeled C1) were recorded by removing the microneedles from the skin at set intervals and imaging them utilizing a stereomicroscope (Fig. 5a). Dissolution of the microneedles could be observed as short as 15 s after insertion into porcine skin (Fig. 5a). More than 95% dissolution of the microneedles could be observed after 5 min (Fig. 5a). After 15 min of introduction to porcine skin, the majority of the microneedle base was also dissolved (data not shown). The quick dissolving capability of these patches allow for rapid administration of C1 to the skin. Patches can be applied and held in place using the Tegaderm patch, and then removed after only a few minutes, making administration extremely fast and easy.

Fluorescent images were then taken of the needle marks on the porcine skins (Fig. 5c). Appearance of rhodamine fluorescence indicates that C1 was successfully implanted into the skin. The fluorescence pattern of rhodamine labeled C1 in skin is nearly identical to the original dimensions of the microneedle patch (Fig. 5b). Due to the elasticity of porcine skin, boundary displacement or tenting of the skin tissue occurs when microneedles are applied to it. Therefore in some area, the needles may not penetrate uniformly, and distances between penetration sites may not equate to distances between needles within the patch. Porcine skin penetration experiment was repeated with 1, 2, 4, 8% C1 microneedles to evaluate their penetration efficiency. All the microneedles contain 1% of rhodamine labeled C1. For 2, 4, 8% C1 microneedles, 1% labeled C1 was mixed with unlabeled C1 to reach the final concentrations. This enables comparison of penetration efficiency, not total protein delivery. Each distinct fluorescent needle mark is counted as a penetration site. The penetration efficiency was quantified as the number of needles penetrated/total number of needles (mean ± SD, $n = 3$) (Supplementary Fig S2). The penetration efficiency decreases as the percentage of collagen increases. An inspection of the microneedles under microscope revealed that increasing collagen content results in more defective needles. The collagen content may also affect the mechanical strength of the needles. Images showing the penetration pattern were also presented (Supplementary Fig S2). Although the penetration efficiency of 2% C1 microneedle is not statistically different from 1% C1 microneedle, we found the 1% needle gave more consistent and uniform delivery. It is possible that even with low penetration efficiency, higher percent C1 microneedles may achieve comparable or higher total protein delivery. However, uniform delivery is crucial in this application. Low penetration efficiency of higher percent C1 microneedle also means more loss of the collagen material, therefore driving up the cost. For these reasons, we decided to use 1% C1 microneedle for the rest of the study.

Although the topical appearance of rhodamine indicates microneedle penetration, it is possible that the needles could just deform the skin, thereby creating a pocket without actually penetrating. To confirm penetration of the microneedles into the porcine skin, application sites were stained with Trypan Blue (Fig. 5d). Trypan blue stains damaged tissue and cells, indicating successful penetration through the stratum corneum and into the epidermis. These results suggest that the microneedles are capable of successfully penetrating through the stratum corneum into the epidermis.

Recent studies have shown that a greater spacing may prove to be optimal.[18] To test the hypothesis that decreasing needle density will increase the force per needle resulting in more efficient or deeper penetration, we also prepared 12 × 6 and 6 × 6 patches (with all the microneedles distributed in the same 0.6 × 0.6 cm area) in addition to the 12 × 12 patch (Fig. 6b). To more accurately quantify the level of C1 delivery to various depths of the porcine skin, skin samples were embedded in OCT compound and sectioned into 25 μm sections parallel to the surface of the skin (Fig. 6a). Different compression and elastic properties within the porcine skin result in differential penetration for every needle. While some needles only penetrate a few tens of microns, some needles were capable of penetrating to 300 μm. When needle density decreased to 6 × 6, the total fluorescence at different depth decreased to ~1/2 but not 1/4 of the level achieved by 12 × 12 patch, indicating protein delivery per needle is more efficient at 6 × 6 density (Fig. 6c). However, the same effect is not seen at 12 × 6 density suggesting that the increment of force per needle at this density is not sufficient to affect needle penetration and protein delivery.

Human Foreskin Collagen I Application

The penetration of C1 (1% 12 × 12) microneedles with rhodamine labelled collagen to human foreskin was tested in a similar manner as can be found in Sun *et al.*[30] Briefly, the foreskin was stretched and pinned to a piece of Styrofoam. The microneedles were attached to an adhesive bandage, and pressed onto the foreskin, where they were left to dissolve. The foreskin was then frozen in OCT Compound, cut into 10–25 μm sections, and stained for imaging.

Fluorescence microscopy examination following application of a 1% C1 microneedle patch illustrated a successful application. The epidermis can be identified as the dense layer of nuclei stained *via* DAPI. Invagination of the epidermis occurs at the points of contact with the microneedles, leading to compression. Red staining is indicative of the rhodamine labelled C1 that was delivered *via* the microneedle patches. Red staining within the nucleated areas of the section indicates that the microneedles were able to penetrate deep into the dermis. In fact, collagen was well established beyond a depth of 100 μm (Figs. 7a–7c).

The area that connects the epidermis to the dermis is known as the basement membrane. The basement membrane is the border between the tightly packed epidermal keratinocytes and the much less densely crowded area of the papillary dermis. Many large proteins and peptides that can freely diffuse through the dermis are restricted from doing so in the epidermis due to the sheer density of cells as well as the presence of desmosomes. Thus, for the delivery of large molecules that target basal keratinocytes, the basement membrane,

fibroblasts, or other sites in the lower epidermis or dermis, it is essential that the microneedles have the ability to penetrate all the way through to the dermis. Staining of the basement membrane laminin 332 reaffirms the ability of the microneedles to penetrate through the epidermal layer and deposit C1 well into the papillary dermal layer (Fig. 7d).

The spacing of the invaginations within the epidermis can be seen in Fig. 7(c). This spacing is almost identical to the spacing seen on the microneedle patch prior to application. The pliability and movement of the skin during microneedle application make it impossible to have a completely uniform and evenly spaced C1 delivery. However, the variation in microneedle penetration spacing is on the scale of tens of microns, resulting in much more evenly distributed C1 than would be obtained *via* an intradermal syringe injection.

Red staining on top of the epidermis indicates that some rhodamine labelled C1 remained on the surface of the foreskin. This is most likely derived from the base part of the patch, and not from the microneedle portions themselves. It is possible to create microneedles that only contain the delivered molecule in the needle portion of the patch, and not in the base portion. [29] However, many of the techniques used to do so involve using high temperatures or UV curation in the process. These conditions can cause the denaturation of many proteins, C1 included. We attempted to create microneedles that only contained C1 in the needles and not in the base at room temperature so as to avoid denaturing conditions. We first poured PVP with 1% C1 into the needle portion of the mold and allowed it to dry. We then poured pure PVP solution over the needles and allowed that to dry to form the base. However, the pure PVP solution dissolved the 1% C1 PVP in the needles, thus allowing the C1 to diffuse throughout the entire patch. Because of this, and due to the relatively low cost of C1, we decided to use 1% C1 solution for the entire patch. For more precious cargo, alternative methods must be used.

DISCUSSION

The results of our experiments illustrate the capability of our microneedle delivery systems to deposit C1 into porcine and human skin. Dissolution of the microneedles occurred within 5 min of application, and fluorescent imaging illustrated that the C1 was deposited deeply into the papillary dermis of the tissue. This shows the speed and effectiveness associated with microneedle application.

For cosmetic collagen applications, the average cost in 2009 was between $480 and $510, without taking into account facility, medication, and anesthesia costs.[31] Currently, techniques are being developed with which recombinant human collagen can be mass produced using tobacco plants.[28] Combining mass produced collagen with a mass produced C1 microneedle delivery system distributed for at-home application could prove to be a very popular venture.

Additionally, the use of C1 microneedles can significantly help reduce the time required in wound healing. Collagen serves as a substrate that promotes cellular proliferation and differentiation.[25] Instead of applying the collagen superficially as current bandages do, microneedles have the ability to apply collagen relatively deep into the dermis, which could

serve to greatly aid in the recruitment of fibroblasts and keratinocytes, greatly expediting the healing process.

In addition to cosmetic improvement and wound healing, microneedle based collagen delivery can provide other advantageous results. Collagen can serve to indirectly enhance the activity of monocyte-derived dendritic cells, thus helping to strengthen the human immune system.[24] Implants of collagen VII may result in the healing of dystrophic epidermolysis bullosa, a disease which results from a lack of type VII collagen in the basement membrane.[11,21,32] Our microneedles have shown their ability to deliver C1 up to and beyond the basement membrane zone. Thus, it is likely that microneedles containing type VII collagen will be able to do the same, healing one of pediatrics' worst dermatological diseases.

CONCLUSION

The use of PVP microneedle delivery systems to transport C1 into human skin is an easy, safe, and effective procedure, which may allow even distribution of C1 to the region of interest. C1 microneedles can be constructed in a short amount of time, and do not adversely affect the structure and function of the protein. Its benefits include cosmetic care, wound healing, and perhaps even enhanced immune-capability and the cure of diseases such as dystrophic epidermolysis bullosa. The superior characteristics of this method of C1 delivery compared to the traditional techniques (e.g., injection), may open up a profitable market specifically in regard to the cosmetic applications in which the stress-free and at-home administration of C1 is important.

Supplementary Material

Refer to Web version on PubMed Central for supplementary material.

Acknowledgments

This work was supported by the National Center for Research Resources and the National Center for Advocacy Translational Sciences, National Institutes of Health, through UL1 TR000093 (formerly UL1 RR025744) and SPARK, Spectrum—the Stanford Center for Clinical and Translational Research and Education; the Stanford NIH/NCCR Clinical Translational Science Award grant number TL1 RR025742, and the Office of Research and Development, Palo Alto VA Medical Center.

ABBREVIATIONS

CD	Circular dichroism
C1	Type-I collagen
DAPI	4′,6-Diamidino-2-phenylindole
MES	Morpholino ethanesulfonic acid
MMP-1	Matrix metallopeptidase 1
MWCO	Molecular weight cut off

OCT	Optimum cutting temperature
PDMS	Polydimethylsiloxane
PEG	Polyethylene glycol
PVP	Polyvinylpyrrolidone
RBITC	Rhodamine B isothiocyanate
SEM	Scanning electron microscopy
Si	Silicon
UVA	Ultraviolet-A

References

1. Al-Zahrani S, Zaric M, McCrudden C, Scott C, Kissenpfennig A, Donnelly RF. Microneedle-mediated vaccine delivery: harnessing cutaneous immunobiology to improve efficacy. Expert Opin Drug Deliv. 2012; 9:541–550. [PubMed: 22475249]
2. Barbero AM, Frasch HF. Pig and guinea pig skin as surrogates for human *in vitro* penetration studies: a quantitative review. Toxicol In Vitro. 2009; 23:1–13. [PubMed: 19013230]
3. Ben Simon GJ, McCann JD. Cosmetic eyelid and facial surgery. Surv Ophthalmol. 2008; 53:426–442. [PubMed: 18929758]
4. Castelo-Branco C, Pons F, Gratacos E, Fortuny A, Vanrell JA, Gonzalez-Merlo J. Relationship between skin collagen and bone changes during aging. Maturitas. 1994; 18:199–206. [PubMed: 8015503]
5. Chilcott RP, Jenner J, Hotchkiss SA, Rice P. *In vitro* skin absorption and decontamination of sulphur mustard: comparison of human and pig-ear skin. J Appl Toxicol. 2001; 21:279–283. [PubMed: 11481660]
6. De Paepe A, Malfait F. The Ehlers–Danlos syndrome, a disorder with many faces. Clin Genet. 2012; 82:1–11. [PubMed: 22353005]
7. Di Lullo GA, Sweeney SM, Korkko J, Ala-Kokko L, San Antonio JD. Mapping the ligand-binding sites and disease-associated mutations on the most abundant protein in the human, type I collagen. J Biol Chem. 2002; 277:4223–4231. [PubMed: 11704682]
8. Dick IP, Scott RC. Pig ear skin as an *in vitro* model for human skin permeability. J Pharm Pharmacol. 1992; 44:640–645. [PubMed: 1359086]
9. Doillon CJ, Silver FH. Collagen-based wound dressing: effects of hyaluronic acid and fibronectin on wound healing. Biomaterials. 1986; 7:3–8. [PubMed: 3955155]
10. Donnelly RF, Singh TR, Garland MJ, Migalska K, Majithiya R, McCrudden CM, Kole PL, Mahmood TM, McCarthy HO, Woolfson AD. Hydrogel-forming microneedle arrays for enhanced transdermal drug delivery. Adv Funct Mater. 2012; 22:4879–4890. [PubMed: 23606824]
11. Epstein EH Jr. Molecular genetics of epidermolysis bullosa. Science. 1992; 256:799–804. [PubMed: 1375393]
12. Greenfield NJ. Using circular dichroism spectra to estimate protein secondary structure. Nat Protoc. 2006; 1:2876–2890. [PubMed: 17406547]
13. Hirobe S, Azukizawa H, Matsuo K, Zhai Y, Quan YS, Kamiyama F, Suzuki H, Katayama I, Okada N, Nakagawa S. Development and clinical study of a self-dissolving microneedle patch for transcutaneous immunization device. Pharm Res. 2013; 30:2664–2674. [PubMed: 23775442]
14. Jian J, Pelle E, Yang Q, Pernodet N, Maes D, Huang X. Iron sensitizes keratinocytes and fibroblasts to UVA-mediated matrix metalloproteinase-1 through TNF-alpha and ERK activation. Exp Dermatol. 2011; 20:249–254. [PubMed: 20701626]

15. Kim KL, Han DK, Park K, Song SH, Kim JY, Kim JM, Ki HY, Yie SW, Roh CR, Jeon ES, Kim DK, Suh W. Enhanced dermal wound neovascularization by targeted delivery of endothelial progenitor cells using an RGD-g-PLLA scaffold. Biomaterials. 2009; 30:3742–3748. [PubMed: 19394079]
16. Kim SE, Lee JH, Kwon HB, Ahn BJ, Lee AY. Greater collagen deposition with the microneedle therapy system than with intense pulsed light. Dermatol Surg. 2011; 37:336–341. [PubMed: 21342311]
17. Kim YC, Park JH, Prausnitz MR. Microneedles for drug and vaccine delivery. Adv Drug Deliv Rev. 2012; 64:1547–1568. [PubMed: 22575858]
18. Kochhar JS, Quek TC, Soon WJ, Choi J, Zou S, Kang L. Effect of microneedle geometry and supporting substrate on microneedle array penetration into skin. J Pharm Sci. 2013; 102(11):4100–4108. [PubMed: 24027112]
19. Mahadevan G, Sheardown H, Selvaganapathy P. PDMS embedded microneedles as a controlled release system for the eye. J Biomater Appl. 2013; 28:20–27. [PubMed: 22262574]
20. Myers BA, Dubick MA, Reiser KM, Gerriets JE, Last JA, Rucker RB. Ozone exposure, food restriction and protein deficiency: changes in collagen and elastin in rodent lung. Toxicol Lett. 1984; 23:43–49. [PubMed: 6485017]
21. Nystrom A, Velati D, Mittapalli VR, Fritsch A, Kern JS, Bruckner-Tuderman L. Collagen VII plays a dual role in wound healing. J Clin Invest. 2013; 123:3498–3509. [PubMed: 23867500]
22. Patel SR, Berezovsky DE, McCarey BE, Zarnitsyn V, Edelhauser HF, Prausnitz MR. Targeted administration into the suprachoroidal space using a microneedle for drug delivery to the posterior segment of the eye. Invest Ophthalmol Vis Sci. 2012; 53:4433–4441. [PubMed: 22669719]
23. Pazzaglia UE, Congiu T, Brunelli PC, Magnano L, Benetti A. The long bone deformity of osteogenesis imperfecta III: analysis of structural changes carried out with scanning electron microscopic morphometry. Calcif Tissue Int. 2013; 93(5):453–461. [PubMed: 23929220]
24. Poudel B, Yoon DS, Lee JH, Lee YM, Kim DK. Collagen I enhances functional activities of human monocyte-derived dendritic cells via discoidin domain receptor 2. Cell Immunol. 2012; 278:95–102. [PubMed: 23121981]
25. Ruszczak Z. Effect of collagen matrices on dermal wound healing. Adv Drug Deliv Rev. 2003; 55:1595–1611. [PubMed: 14623403]
26. Sachs DL, Rittie L, Chubb HA, Orringer J, Fisher G, Voorhees JJ. Hypo-collagenesis in photoaged skin predicts response to anti-aging cosmeceuticals. J Cosmet Dermatol. 2013; 12:108–115. [PubMed: 23725304]
27. Sadick NS, Karcher C, Palmisano L. Cosmetic dermatology of the aging face. Clin Dermatol. 2009; 27:S3–S12.
28. Shoseyov O, Posen Y, Grynspan F. Human recombinant type I collagen produced in plants. Tissue Eng Part A. 2013; 19:1527–1533. [PubMed: 23252967]
29. Sullivan SP, Murthy N, Prausnitz MR. Minimally invasive protein delivery with rapidly dissolving polymer microneedles. Adv Mater. 2008; 20:933–938. [PubMed: 23239904]
30. Sun W, Araci Z, Inayathullah M, Manickam S, Zhang X, Bruce MA, Marinkovich MP, Lane AT, Milla C, Rajadas J, Butte MJ. Polyvinylpyrrolidone microneedles enable delivery of intact proteins for diagnostic and therapeutic applications. Acta Biomater. 2013; 9:7767–7774. [PubMed: 23648574]
31. Surgeons ASOP. Dermal fillers: collagen minimally invasive procedure. Coscmetic Procedures. 2012
32. Wang X, Ghasri P, Amir M, Hwang B, Hou Y, Khilili M, Lin A, Keene D, Uitto J, Woodley DT, Chen M. Topical application of recombinant type VII collagen incorporates into the dermal–epidermal junction and promotes wound closure. Mol Therapy. 2013; 21:1335–1344.
33. Wild T, Rahbarnia A, Kellner M, Sobotka L, Eberlein T. Basics in nutrition and wound healing. Nutrition. 2010; 26:862–866. [PubMed: 20692599]

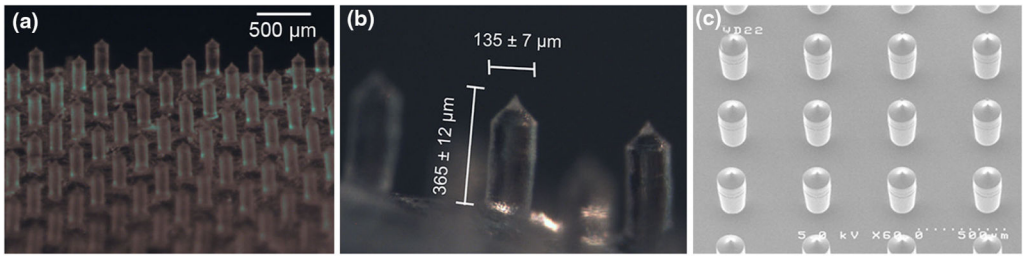

FIGURE 1.

(a) Bright field image of microneedles patch showing array of microneedles. (b) Bright field image illustrating the dimensions of a single needle within the microneedle patch. (c) SEM images of the silicon positive mold used to make PDMS negative mold.

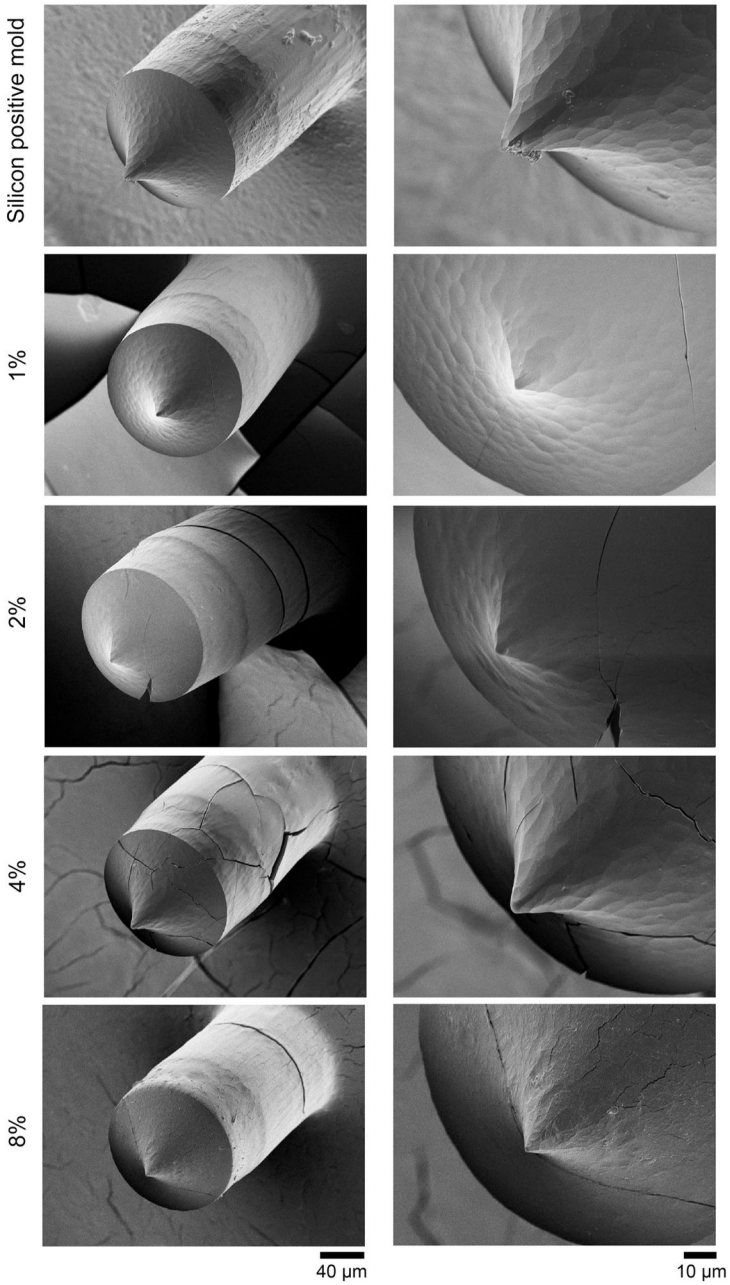

FIGURE 2.

SEM images of silicon needle and PVP-C1 microneedles with different C1 content, 1, 2, 4, 8% C1/PVP (w/w). The cracking was likely caused by the coating process performed in the vacuum sputter coater before SEM images were taken.

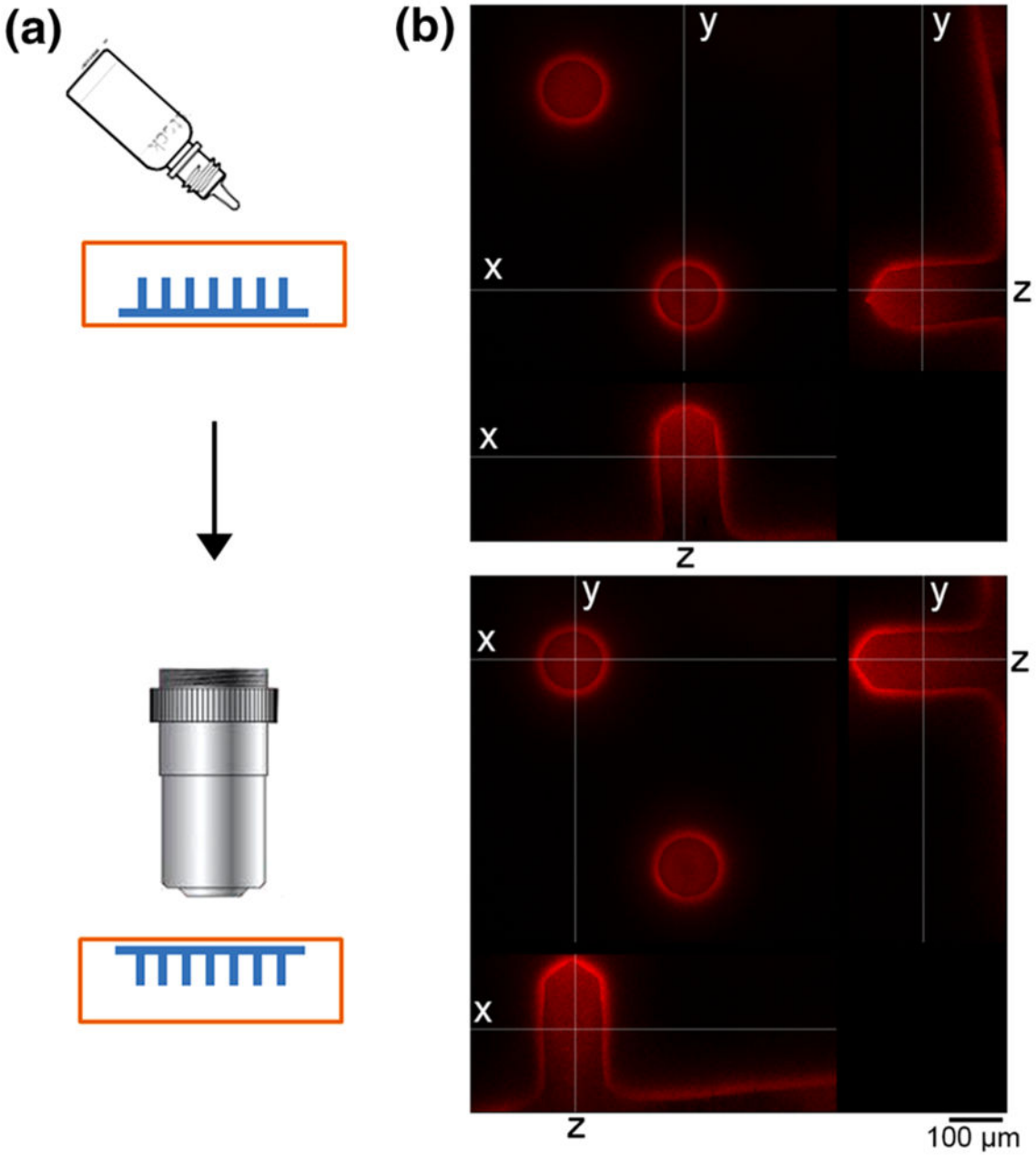

FIGURE 3.

(a) Scheme showing the embedding of microneedles in resin and imaging. (b) Confocal images of two rhodamine labeled PVP-C1 microneedles at **x**, **y** and **z** optical sections.

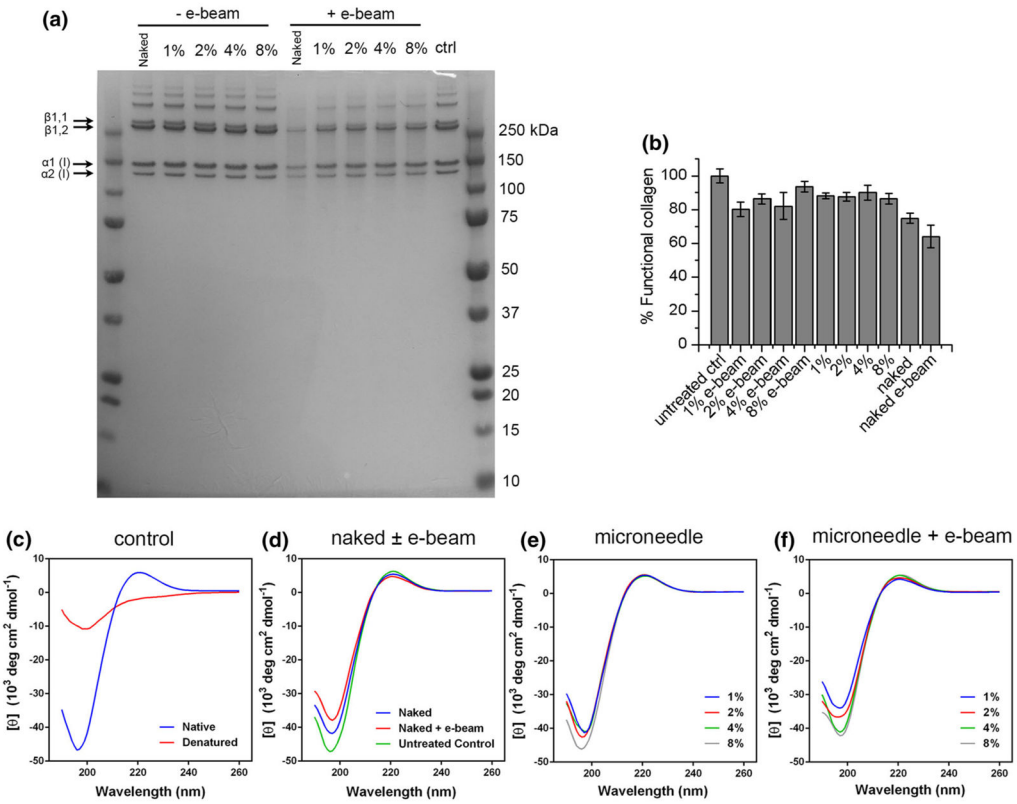

FIGURE 4.

(a) SDS PAGE showing naked C1 and C1 recovered from PVP-C1 microneedles patch made with 1, 2, 4, 8% C1 (w/w) with and without e-beam treatment. Control is untreated collagen in 50 mM MES buffer (pH 6.0). (b) Concentrations of functional collagen were determined by rat type I collagen specific ELISA. Results are presented as % functional collagen compared to untreated controls (mean ± SD, **n** = 3). (c) CD spectra of C1 as controls, native conformation at 4 °C and denatured at 60 °C. (d) CD spectra of untreated control, air dried naked C1 with and without e-beam treatment. (e) CD spectra of C1 recovered from 1, 2, 4, 8% microneedles after preparation without e-beam treatment. (f) CD spectra of C1 recovered from 1, 2, 4, 8% microneedles that were subjected to e-beam sterilization.

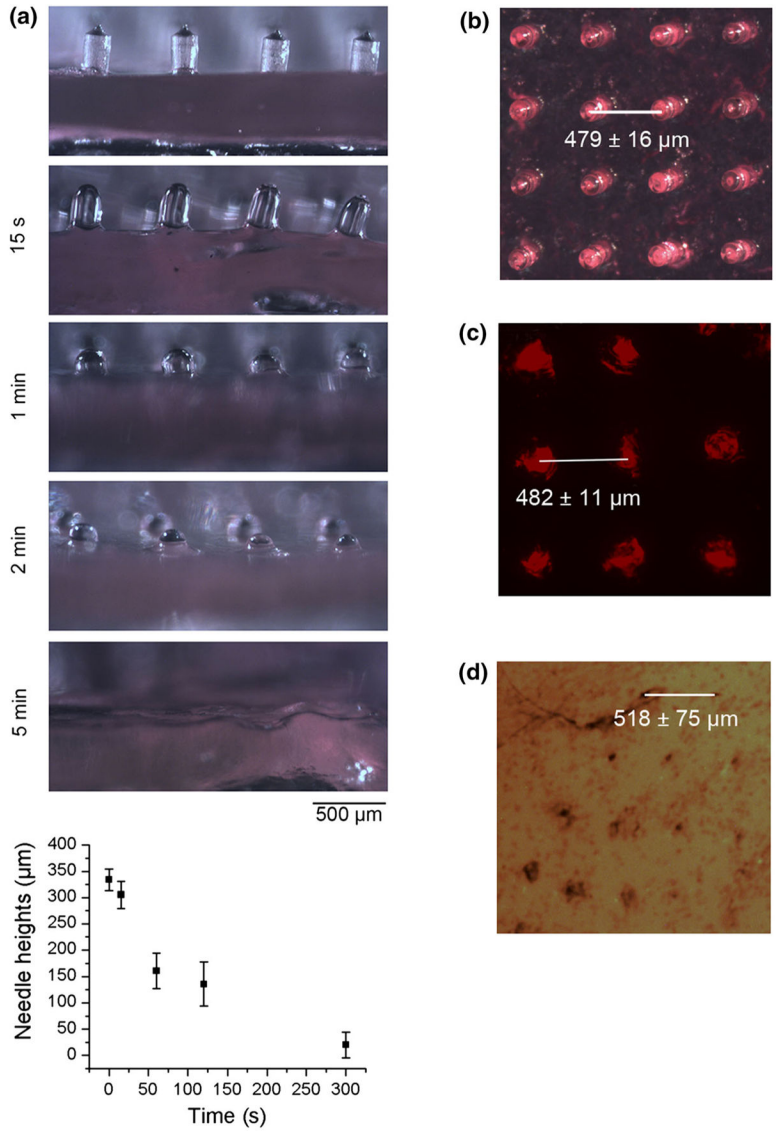

FIGURE 5.

(a) Images of PVP-C1 microneedles before and after 15 s, 1, 2 and 5 min, insertion into porcine skins. Lower panel shows quantification of needle heights at different time points. The heights of 15–20 needles were measured and the experiment were repeated three times. (b) Image of rhodamine labeled microneedles. (c) Fluorescent image of needle marks in porcine skin. (d) Needle marks on porcine skin after Trypan blue staining.

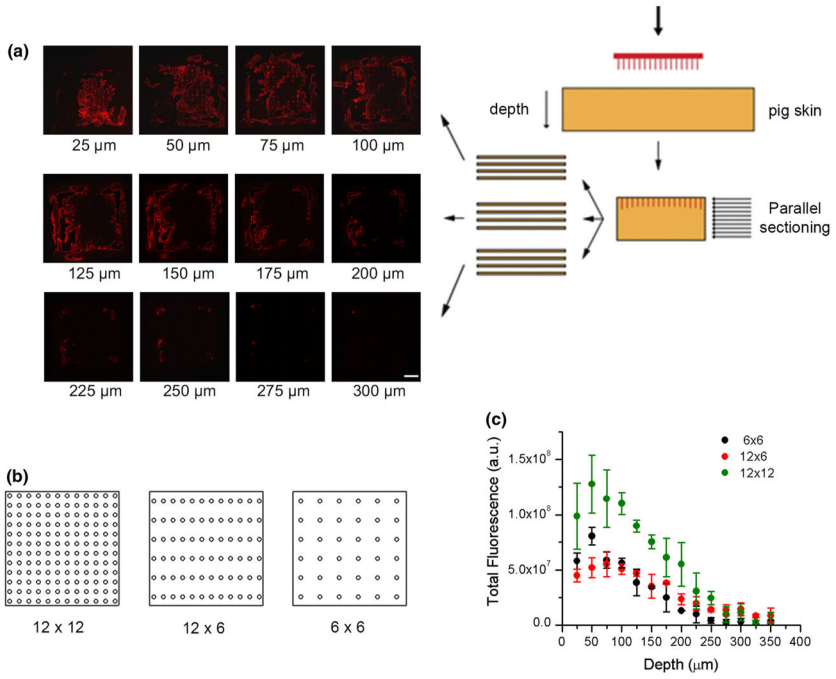

FIGURE 6.

Pig skin was punctured with PVP microneedle containing rhodamine labeled C1. Needle patch has standard size of 0.6 × 0.6 cm with 12 × 12, 12 × 6 and 6 × 6 needle density. Cryosectioning was performed parallel to the surface. (a) Representative fluorescent images for each 25 μm layers of porcine skin penetrated by a 12 × 12 microneedle patch. Scale bar = 500 μm. (b) Graphical representation of microneedle patches with different densities. (c) Total fluorescence was quantified for each 25 μm section and plotted against depth.

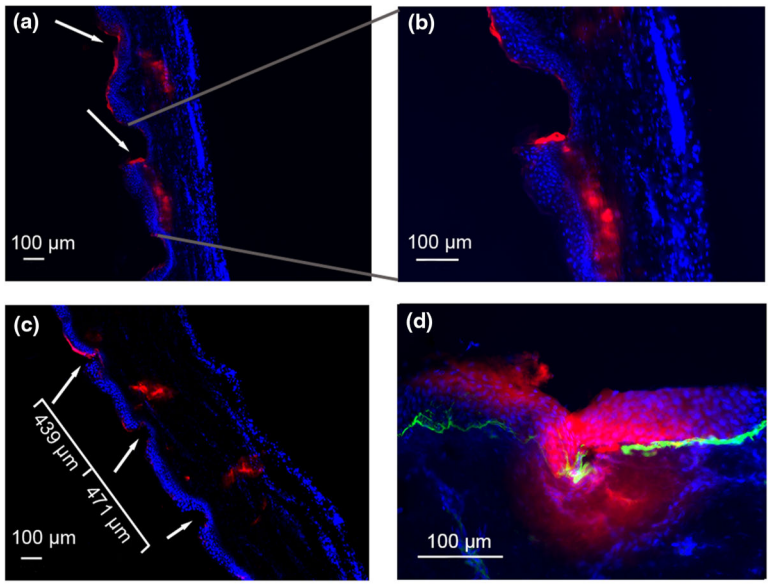

FIGURE 7.

Fluorescent images of rhodamine labeled PVP-C1 penetrating human foreskins. Epidermis is on the left in (a, b, and c) Epidermis is on top in (d) Red, rhodamine fluorescence; blue, DAPI staining; green (panel d), laminin 332.